sustainability

MDPI

Article

Multi-Objective Optimal Power Flow Calculation Considering Carbon Emission Intensity

Gangfei Wang [1], Hengrui Ma [1,2,3,*], Bo Wang [2,3], Abdullah M. Alharbi [4], Hongxia Wang [3,5] and Fuqi Ma [2,3,6]

1 College of Energy and Electrical Engineering, Qinghai University, Xining 810016, China; wgangfei@163.com
2 Hubei Engineering and Technology Research Center for AC/DC Intelligent Distribution Network, School of Electrical Engineering and Automation, Wuhan University, Wuhan 430072, China; whwdwb@whu.edu.cn (B.W.); whumfq@whu.edu.cn (F.M.)
3 School of Electrical and Automation, Wuhan University, Wuhan 430072, China; 2018282070092@whu.edu.cn
4 Department of Electrical Engineering, College of Engineering at Wadi Addawasir, Prince Sattam bin Abdulaziz University, Wadi Addawasir 11991, Saudi Arabia; am.alharbi@psau.edu.sa
5 Department of Electrical & Computer Engineering, University of Denver, Denver, CO 80210, USA
6 School of Electrical Engineering, Xi'an University of Technology, Xi'an 710054, China
* Correspondence: henry3764@foxmail.com

Abstract: In keeping with China's dual carbon goals, optimal low-carbon power system dispatch has become a necessary component of the greening of the power system. However, typically, research considers only the economics of such efforts. Based on our power flow analysis of the power grid and the correlation properties of carbon emission flow, an optimal power flow calculation model targeting the total carbon emission rate of the power system's power generation cost, active network loss, and load and network loss was constructed. Next, the NSGA-III algorithm was used to solve the model, and the decision was to coordinate and optimize the output schemes of various types of power plants, such as wind, water, and thermal. The modified IEEE39 node simulation system was built with Matlab software (MATLAB R2020b). The results of the calculation showed that, compared to the traditional method of determining the optimal power flow, the proposed method reduced the system carbon emissions by 20% while the power generation cost increased by less than 2%, which proves the effectiveness and practicability of the proposed method.

Keywords: carbon emission flow; NSGA-III algorithm; optimal power flow; TOPSIS method

Citation: Wang, G.; Ma, H.; Wang, B.; Alharbi, A.M.; Wang, H.; Ma, F. Multi-Objective Optimal Power Flow Calculation Considering Carbon Emission Intensity. *Sustainability* **2023**, *15*, 16953. https://doi.org/10.3390/su152416953

Academic Editors: Xun Shen, Wenlong Fu and Nan Yang

Received: 31 October 2023
Revised: 8 December 2023
Accepted: 12 December 2023
Published: 18 December 2023

1. Introduction

Greenhouse gas emissions (GHG) have emerged as a global concern hindering societal progress. Recognizing this challenge, the international community is unified in its drive to foster the development of a low-carbon economy and enhance the optimization of the energy composition. During the general debate of the 75th session of the United Nations General Assembly on the 22 September 2020, President Xi Jinping of China declared that China is committed to attaining the pinnacle of carbon emissions before 2030 and aims to achieve carbon neutrality by 2060 [1]. As of the conclusion of 2021, China, being one of the largest power consumers, boasted an installed power generation capacity of 2.38 billion kW. Thermal power constituted 56.58% of this total capacity [2]. According to statistics, the power industry's share of national carbon emissions has reached 50% [3]. According to the predictions in the literature [4], the Chinese power sector can achieve the goal of zero carbon dioxide emissions by 2050, with the completion of technology for capturing and storing carbon emissions [5], the transformation of thermal power units, and the utilization of mass renewable energy power generation. The power industry holds immense potential for reducing CO_2 emissions. The transition to a low-carbon power system will greatly promote the realization of China's dual-carbon goals [6]. Therefore, a thorough analysis of carbon emissions, coupled with generation costs, is essential in the operation of power systems. This will allow for the judicious use of renewable power resources [7], driving power systems closer to their low-carbon and economic objectives.

For power systems to realize green and low-carbon electricity dispatch, it is crucial to concurrently weigh the economic and reliability aspects of power dispatching [8] with the system's CO_2 emissions characteristics. In Li and Han [9], second-order Taylor expansion is used to correct the state variables once, and the corrected results are used to calculate the control variables and the output of the distributed energy sources. Using the sparse characteristics of the Hessian array, a distributed Gaussian elimination method is proposed to achieve a distributed solution for the distribution network optimal power flow. Zhang et al. [10], who endeavor to address active network loss, propose a method for optimal power flow calculation with controllable phase shifters based on the improved interior point method. Another relevant study is that of Zhu et al. [11], which establishes an uncertain optimal power flow model for evaluating the absorptive capacity of renewable distributed generation and a deterministic equivalent conversion method for an optimal power flow model under different description forms. Study [12] proposes an optimal power flow solution method for systems integrating solar photovoltaic and wind energy with traditional generators based on the hybrid particle swarm gray wolf optimizer (HPS-GWO). By analyzing the features of coal-fired power plants, Wang et al. [13] formulates a mathematical model depicting the correlation between carbon emissions and generator output, and proposes a dual-objective economical and low-carbon optimal scheduling method employing an algorithm that evolves weights adaptively. However, this broad approach to carbon emissions lacks the capability to analyze individual links within the system. Zhang et al. [14] introduces the cost associated with CO_2 over-emissions and the generalized cost of wind power generation. To account for the influence of carbon emission quotas and the integration of wind power on system power generation costs, a day-ahead scheduling model is formulated, with the optimization objective being the minimization of the overall system power generation cost. Mei et al. [3] uses an aggregate allocation method to fairly allocate carbon emission rights, and then establishes a model for low-carbon electricity dispatch, taking into account the constraints imposed by carbon emission rights. But this allocation model is established on a macro level, and cannot conduct an in-depth analysis of carbon emissions in the power system. Han et al. [15] proposes a power system low-carbon scheduling strategy, taking into account flexible demand response and energy storage by combining a carbon emission index with a flexible resource scheduling model. In Li et al. [16], a dual-layer alternating optimal scheduling model is formulated, encompassing day-ahead dispatch and load demand response [17]. Additionally, in light of carbon capture systems and the theory of carbon emission flow, a low-carbon optimal learning and dispatching method for the power system is introduced. In Zhong et al. [18], a bi-level optimization model is proposed to guide users to actively choose green energy consumption. The higher level seeks to maximize the benefits of wind power, photovoltaic, and coal-fired power plants, and the lower level aims at minimizing the cost of electricity consumption, utilizing electricity prices and carbon responsibility as motivating factors. The carbon emissions in Jiang et al. [19] and Fakih et al. [20] are calculated based on fuel or typical energy carbon emission factors. This study exclusively investigates carbon emissions from the energy supply side and does not conduct an internal analysis of the system.

However, the above studies either only consider the economy and reliability of the power grid, or only analyze macro carbon emissions, and there is no micro study of every unit of the electrical grid. To deal with these problems, this paper optimizes the dispatch of the power system with the goals of economy and environmental protection. According to the unique traits of carbon emission flow, this paper analyzes the virtual carbon emission flow across different sections of the power grid. By establishing an optimal power flow model that prioritizes power generation cost, active network loss, and the overall carbon emission rate, the power generation strategy is devised by maximizing the utilization of renewable resources and reducing their carbon emissions. Finally, this paper takes the modified IEEE-39 node system as a demonstration to validate the efficacy and viability of the proposed approach.

2. Model Design and Calculation of Carbon Emission Flow in Power System

2.1. Carbon Emission Flow of Power System

The carbon emission flow of the power system refers to the flow process of the CO_2 emissions generated during the production, transmission, and use of electricity. The carbon emission features of the power system are that emissions are concentrated at the power generation end and consumption is concentrated at the load end [21]. From the perspective of the energy transfer chain, carbon emissions are collected from the power generation side to the consumer end through the power flow. If the carbon emissions generated in the power production process are regarded as flowable, they flow to the load along with the power flow and are finally discharged into the atmosphere. The distribution of carbon emissions moving through the power system is called the carbon emission flow of the power system [22], which is also referred to as the carbon flow. The carbon flow of the power system is a virtual network flow attached to the power flow. It is shown in Figure 1. Carbon emission flow helps to analyze the carbon emissions of the power system and offers a theoretical foundation for the low-carbon transition of the electricity grid.

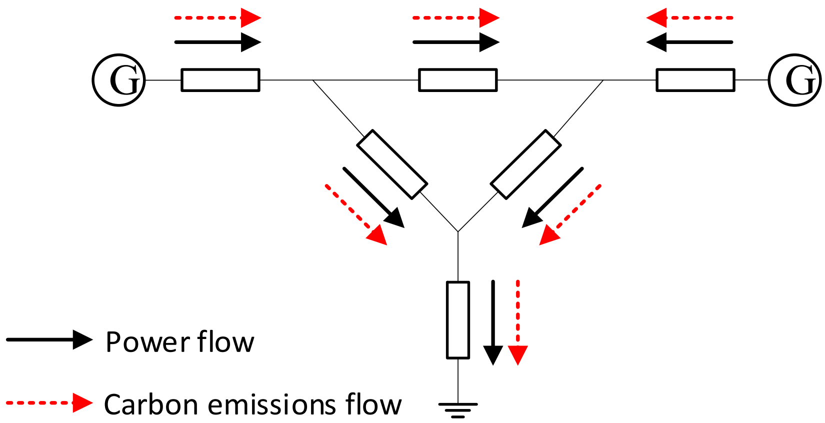

Figure 1. Chart of carbon emission flow in power system. The letter "G" represents the power generation end.

2.2. Basic Definition of Carbon Emission Flow in Power System

The theory of carbon flow in power systems utilizes several new terms that form the theoretical basis for its analysis; these are shown below.

2.2.1. Carbon Emission Flow

Also referred to as carbon flow, this refers to the total quantity of carbon emissions associated with the carbon emission flow traversing a node or branch of the power flow within a specific timeframe by the symbol F, as stated in tCO_2.

2.2.2. Carbon Flow Rate

This indicates the carbon flow passing through a node or branch per unit time. It is represented by the symbol R, as stated in tCO_2/h, which is mathematically equivalent to the derivative value of carbon flow with respect to time.

$$R = \frac{F}{t} \quad (1)$$

where t is time, as stated in hour (h).

2.2.3. Branch Carbon Flow Density

The carbon flow of the electricity grid relies on the power flow. The carbon emissions generated by the generating plant side resulting from the transmission of unit electricity on the branch of the grid are collectively called the carbon flow density of the branch. It is alternatively defined as the proportion of the carbon flow rate to the active power of a branch within the power system. It is denoted by the symbol ρ, measured in units of tCO_2/kWh.

$$\rho = \frac{R}{P} \tag{2}$$

where P is the active power, as stated in kW.

2.2.4. Nodal Carbon Intensity

The carbon emission of the power plant side caused by the consumption of unit electricity at the node side is the node carbon intensity, represented by e, measured in tCO_2/kWh. On the power plant side, the carbon intensity at the node is equivalent to the carbon emission intensity of the power plant.

$$e = \frac{\sum\limits_{i \in N^+} P_i \rho_i}{\sum\limits_{i \in N^+} P_i} = \frac{\sum\limits_{i \in N^+} R_i}{\sum\limits_{i \in N^+} P_i} \tag{3}$$

where N^+ signifies the aggregation of all branches of the power flow directed into the node; i denotes the branch index.

In accordance with the principles of proportional sharing and energy conservation, any outflow power flow branch connected to the node contains all the components of the inflow power flow branch, and the carbon flow rate of the outflow power flow branch is equal to the sum of the carbon flow rates contributed by all the inflow power flow branches to the branch [23]. It can be obtained from (4), where the carbon flow density of all the branches flowing out of the from the node equals the carbon intensity of the node. In (4), ρ_{ij} represents the carbon flow density of the branch from node i to node j, then $\rho_{ij} = e_i$, that is, the carbon flow density of the branch is equivalent to the carbon intensity of the originating node flowing into the branch.

$$\begin{aligned} \rho_{j,j \in N^-} &= \frac{\sum\limits_{i \in N^+} P_j \frac{P_i}{\sum\limits_{s \in N^+} P_s} \rho_i}{P_j} \\ &= \frac{\sum\limits_{i \in N^+} P_i \rho_i}{\sum\limits_{s \in N^+} P_s} = \frac{\sum\limits_{s \in N^+} R_s}{\sum\limits_{s \in N^+} P_s} \\ &= e \end{aligned} \tag{4}$$

2.3. Calculation Method for Carbon Emission Flow in Power System

In the power flow analysis, one can compute the power flow distribution across all nodes and branches. Once the carbon potential of each node is known, the carbon emission flow rate for each branch can be determined based on the characteristics of the power system's carbon emission flow and the results of the power flow calculations. Subsequently, solving for the entire system's carbon emission flow becomes feasible [23,24]. Therefore, the primary objective in carbon emission flow calculation is the determination of the carbon potential for each node in the power system.

According to the definition of node carbon potential, the carbon potential of node n is:

$$e_n = \frac{\sum\limits_{i \in N^+} P_{Bi} \rho_i + P_{Gn} e_{Gn}}{\sum\limits_{i \in N^+} P_{Bi} + P_{Gn}} \tag{5}$$

where P_{Bi} conveys the real power from branch i directed into node n, measured in kW; P_{Gn} denotes the real power injected by the power plant to node n, measured in kW; e_{Gn} represents the carbon emission intensity of generators at node n, with units of CO_2/kWh; and ρ_i denotes the branch carbon flow density of branch i, measured in tCO_2/kWh.

2.4. Correlation Analysis between Power Plant and Node Carbon Flow, Load Carbon Flow

As was established by [25], the carbon flow output distribution factor is equal to the power flow output distribution factor. The two are collectively referred to as the node output distribution factor.

$$H_{ij} = H_{ij}^F = H_{ij}^P = \frac{R_{ij}}{\sum R_i} = \frac{P_{ij}}{\sum P_i} \tag{6}$$

where H_{ij}, H_{ij}^F, and H_{ij}^P are node output distribution factors, carbon flow output distribution factors, and power flow output distribution factors from node i to node j, respectively; R_{ij} is the carbon flow rate from node i to node j; $\sum R_i$ represents the total carbon flow inflow from node i; P_{ij} denotes the active power flow flowing from node i to node j; and $\sum P_i$ is the total active power flow flowing into node i.

The path output distribution factor is determined by the proportion of the network flow departing from the source node compared to the total network flows entering the destination node [24]. Specifically, the path transmission distribution factor D_{ij} signifies the flow distribution from node i to node j.

$$D_{ij} = \sum_{L \in \gamma} \Big(\prod_{(m,n) \in B_L} H_{m,n} \Big) \tag{7}$$

where (m, n) is a branch from node m to node n on the path L; B_L is a path from node i to node j; and γ is a set of paths from node i to node j.

$R_{Gk,i}$ represents the contribution of power plant k to the carbon flow rate at node i.

$$R_{Gk,i} = P_{Gk} e_{Gk} D_{ki} \tag{8}$$

where P_{Gk} denotes the real power produced by power plant k; and e_{Gk} is the carbon emission intensity of power plant k.

$R_{Gk,Li}$ represents the contribution of power plant k to the carbon flow rate at load i.

$$R_{Gk,Li} = R_{Gk,i} \frac{P_{Li}}{\sum P_i} \tag{9}$$

where P_{Li} is the real power consumption of load i; and $\sum P_i$ is the cumulative real power flow directed into node i.

In essence, following the principles of carbon emission flow theory, the carbon emission flow and carbon flow rate align with electricity and active power within the power flow context, respectively, bearing distinct physical interpretations. By formulating the theoretical framework of carbon emission flow, it becomes possible to compute the carbon emissions attributable to both load consumption and branch transmission within the system. This calculation relies on the power generation output and the power flow within the grid. Consequently, the original carbon emissions attributed solely to power generation are effectively distributed across various segments of the power system, adhering to a specific mechanism. This allocation provides a foundational framework for scrutinizing carbon emissions across the different segments of the power grid.

3. Optimal Power Flow Considering Carbon Emission Rate

As depicted in (10), the optimal power flow problem is a constrained optimization problem [26] which can be described as: under the condition that the network structure and parameters and the system load are given, various equality and inequality constraints [27, 28] are satisfied, and one or several given objective functions describing the operating efficiency of the system are maximized, by determining the controllable variables of the system.

$$\begin{cases} \quad min(f(u,x)) \\ s.t. \quad g(u,x) = 0 \\ \quad h(u,x) \le 0 \end{cases} \tag{10}$$

where $min\ f(u,x)$ is the objective function; $g(u,x) = 0$ is the equality constraint; $h(u,x) \le 0$ is the inequality constraint; u is the controllable variable, which usually includes the real power output and reactive power output (or terminal voltage) of each power plant, the tap position of the phase shifter, and the tap position of the voltage regulator; and x represents the state variable and the dependent variable of the controllable variable, which usually includes the node voltage and the power of each branch.

3.1. Objective Function

This paper studies the multi-objective optimal power flow in the power grid considering carbon emission intensity. The objectives include the lowest system power generation cost, the smallest real network loss, and the lowest total carbon flow rate. The mathematical model for each objective function is expressed as follows:

1. Lowest cost of power generation:

$$min \sum_{i=1}^{N_{gen}} (a_{i1}P_{Gi} + a_{i0}) \tag{11}$$

where N_{gen} denotes the total number of power plants; P_{Gi} denotes the real power produced by power plant i; and a_{i1} and a_{i0} refer to the cost characteristic coefficients of power plant i.

2. The lowest active network loss:

$$min \sum_{(i,j) \in n_b} P_{ij} + P_{ji} \tag{12}$$

where n_b is the collection of all branches.

3. The lowest total carbon flow rate:

$$min(\sum_{i \in n_l} R_{Li} + \sum_{i \in n_b} R_{Biloss}) \tag{13}$$

where n_l is the collection of all loads; R_{Li} represents the carbon flow rate consumed by the load i; and R_{Biloss} indicates the carbon flow rate consumed by the real power loss on branch i.

3.2. Constraints

3.2.1. Equality Constraints

As depicted in (14) and (15), the optimal power flow denotes an optimized distribution of power flow, where adherence to the equality constraints of the fundamental power flow equations is necessary [29]. Additionally, considering the direction of the carbon flow from the power generation side to the consumer end for consumption, it is essential to maintain equilibrium between the injection and consumption of carbon emission flow.

$$P_{Gi} - P_{Li} - U_i \sum_{j=1}^{n} U_j (G_{ij} \cos\theta_{ij} + B_{ij} \sin\theta_{ij}) = 0 \tag{14}$$

$$Q_{Gi} - Q_{Li} - U_i \sum_{j=1}^{n} U_j (G_{ij} \sin\theta_{ij} - B_{ij} \cos\theta_{ij}) = 0 \tag{15}$$

$$R_{Gi} - R_{Li} - \sum_{\substack{j=1 \\ j \neq i}}^{n} R_{ij,loss} = 0 \tag{16}$$

where n denotes the total number of nodes in the power grid; P_{Gi} and Q_{Gi} are the real power and reactive power generated by the power plant i, respectively; P_{Li} and Q_{Li} are the real load and reactive load at the bus i, respectively; G_{ij} and B_{ij} are the real part and imaginary part of the element in row i and column j of the node admittance matrix, respectively; θ_{ij} is the phase difference between node i and node j, $\theta_{ij} = \theta_i - \theta_j$; U_i and U_j are amplitudes of voltage at node i and node j, respectively; R_{Gi} is the carbon flow rate injected into the system by power plant i; R_{Li} is the carbon flow rate consumed by the load of bus i; and $R_{ij,loss}$ denotes the carbon flow rate of the network loss from node i to node j.

3.2.2. Inequality Constraints

To ensure the secure and reliable operation of the power system, the power plant is mandated to adhere to its operational upper and lower limits [30]. In addition, the voltage amplitudes and line capacities need to meet some requirements.

$$P_{Gi,\min} \leq P_{Gi} \leq P_{Gi,\max} \tag{17}$$

$$Q_{Gi,\min} \leq Q_{Gi} \leq Q_{Gi,\max} \tag{18}$$

$$U_{i,\min} \leq U_i \leq U_{i,\max} \tag{19}$$

$$S_{ij} \leq S_{ij,\max} \tag{20}$$

where $P_{Gi,min}$ and $P_{Gi,max}$ are the upper and lower limits of the active power generated by the i-th generator; $Q_{Gi,min}$ and $Q_{Gi,max}$ are the upper and lower limits of the reactive power generated by the i-th generator; $U_{i,min}$ and $U_{i,max}$ are the upper limit and lower limit of the voltage amplitude of node i, respectively; and $S_{ij,max}$ denotes the upper limit of the line capacity of the branch from node i to node j.

3.3. Optimal Model Solution

3.3.1. NSGA-III Algorithm

NSGA-III (Non-dominated Sorting Genetic Algorithm III) is a multi-objective optimization algorithm, which is an improvement and extension of the classic NSGA-II algorithm [31]. The structure of NSGA-III closely mirrors that of NSGA-II, incorporating swift non-dominated sorting to categorize individuals within the population into distinct, non-dominated fronts. The divergence lies in the environmental selection within the critical layer, where NSGA-II preserves diversity through crowding comparison. The most significant alteration in NSGA-III involves the utilization of the minimum habitat mechanism to select optimal individuals through evenly distributed reference points to preserve population diversity [32]. The flowchart of the NSGA-III algorithm is illustrated in Figure A1 included in Appendix A. The implementation of NSGA-III is as follows:

1. Initialization. Set the basic variables of the NSGA-III algorithm, including the population size, mutation probability, number of iterations, and crossover probability, etc. Read the node, branch, and power plant data of the power grid. The initial population is obtained according to the constraints of the decision variables and the fitness function. Create a population archive set S.
2. Genetic manipulation. Perform selection, crossover, and mutation operations on the parental population to generate the offspring population Q.

3. Non-dominated sorting stratification. Merge the parental and offspring populations and execute fast non-dominated sorting, stratify according to the dominance level of the individual, and then put the individual into the archive set S layer by layer until the amount of individuals in set S is not less than the population size.
4. Selection of individuals in the critical layer based on reference point. In the NSGA-III algorithm, diversity within the population is preserved by incorporating evenly spread reference points. These reference points are utilized to choose individuals situated in the crucial layer, preventing the optimization process from being trapped in local optima. The pivotal layer within the archive set "S" is referred to as the "critical layer." Assuming this layer is denoted as the "L-th" layer, the objective is to select "K" individuals from this critical layer (where "K" equals the population size minus the count of individuals present in the preceding "L − 1" layers within set "S"). These chosen individuals from the critical layer, along with individuals from the "L − 1" layer, together constitute a fresh population set.
5. Continue Steps 2 to 4 until the prescribed number of iterations is reached. Finally, output the Pareto front [33].

3.3.2. Pareto Optimal Set Decision Making

In this paper, the importance of each index is highlighted by assigning specific weights to individual objectives. Subsequently, the TOPSIS method is used to evaluate and sort each solution within the Pareto optimal solution set for the selection of the optimal solution [34,35]. The detailed procedure is outlined as follows:

1. Obtain a collection of optimal Pareto solution sets through the NSGA-III algorithm, that is, the indicator matrix $P_{(m,n)}$ (suggesting that there are a total of m solutions, with each solution comprising n indicators), and subsequently allocate a weight α_n to each indicator within the solution set n (indicates that the weight of the nth index is α_n).
2. Standardize the indicator matrix and assign weights to each element to derive the weighting matrix K.

   The standardized index matrix is:

$$\boldsymbol{P}^*(m,n) = \frac{\boldsymbol{P}(m,n)}{max(\boldsymbol{P}(:,n))} \tag{21}$$

   The weighting matrix is:

$$\boldsymbol{K}(m,n) = \boldsymbol{P}^*(m,n) \times \alpha_n \tag{22}$$

3. Consider the minimum element in each column of the weighting matrix as the optimal solution for index n, denoted as P_n^+, and the maximum element as the worst solution for index n, denoted as P_n^-. Compute the distance of each solution in the weighting matrix to the optimal and worst solutions, denoted as, Z_m^+ and Z_m^-, respectively.

$$\begin{cases} Z_m^+ = \sqrt{\sum\limits_{i=1}^{n} \left(\boldsymbol{K}(m,n) - P_n^+\right)^2} \\ Z_m^- = \sqrt{\sum\limits_{i=1}^{n} \left(\boldsymbol{K}(m,n) - P_n^-\right)^2} \end{cases} \tag{23}$$

4. Compute the proximity index R for each solution within the Pareto solution set with respect to the optimal level. Select the solution corresponding to the maximum R value as the objective function value to achieve optimal power flow.

$$R_m = \frac{Z_m^-}{Z_m^+ + Z_m^-} \tag{24}$$

4. Case Studies

4.1. Basic Data

As depicted in Figure 2, this paper validates the proposed method based on a modified IEEE-39 bus system using the Matpower toolbox in MATLAB (MATLAB R2020b). See Tables A2 and A3 included in Appendix A for the bus and branch data of the system. The modified parameters of each power plant are shown in Table A1 included in Appendix A. The benchmark capacity for power flow calculation is 100 MVA. References [36–40] analyze the power generation types, the expense of power generation is justified, and the carbon intensity of each power plant is given. After the modification, the system contains a total of 10 power plants. Among them, G1 and G9 are hydroelectric power generations, G2 and G4 are coal-fired power generations, G3, G6, and G10 are gas-fired power generations, G5 is wind power generations, and G7 and G8 are photovoltaic power generations. The case of this study is pure fiction.

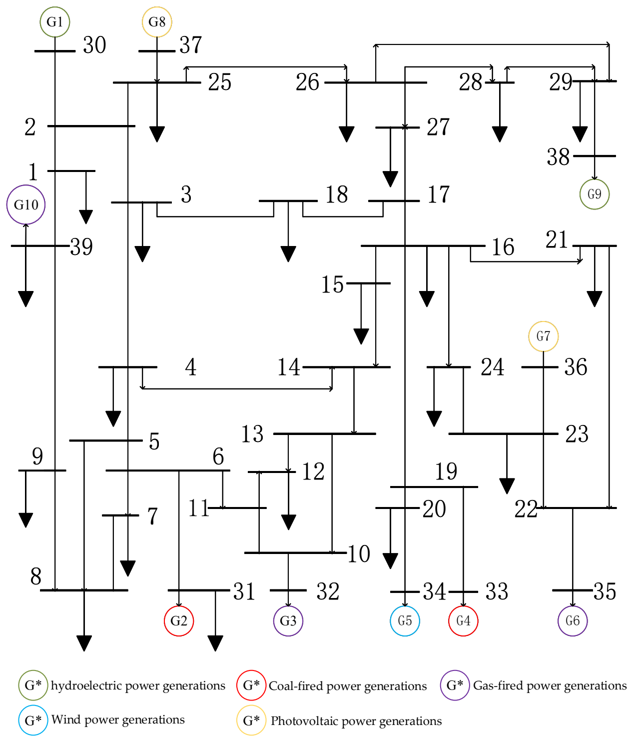

Figure 2. Modified IEEE-39 Bus System.

4.2. Example Setting and Analysis

This paper establishes two scenarios to compare and analyze the electricity generation cost, active network loss, and total carbon flow rate of the system. Scenario 1 is employed for calculating the optimal power flow of the traditional power system. Subsequently, the carbon flow distribution of the system is determined by utilizing the optimal power flow distribution and the characteristics of carbon emission flow. Scenario 2 is used to calculate the Pareto optimal frontier of the three objectives (the power generation cost, the active network loss, and the total carbon flow rate of the grid) through the NSGA-III algorithm and determine the optimal solution using the TOPSIS method.

Scenario 1:

Table 1 depicts the optimal power generation from power plant in the IEEE 39-bus system. Under this power plant output scheme, the power generation cost of the grid is 2.3936 million CNY, the active network loss is 37.698 MW, and the total carbon flow rate is 2.25×10^9 tCO_2/h.

Table 1. The output of power plant under Scenario 1.

Bus	Generation Type	Active Output (MW)	Reactive Output (MVAr)
30	Hydroelectric power generation	534.00	180.64
31	Coal-fired power generation	624.75	251.54
32	Gas-fired power generation	636.91	245.05
33	Coal-fired power generation	603.75	176.16
34	Wind power generation	477.88	126.62
35	Gas-fired power generation	615.99	135.94
36	Photovoltaic power generation	537.97	97.68
37	Photovoltaic power generation	451.70	31.07
38	Hydroelectric power generation	766.98	−6.43
39	Gas-fired power generation	1041.99	44.51

Scenario 2:

Table 2 depicts the basic parameters of the NSGA-III algorithm in Scenario 2, based on which, the Pareto optimal front is obtained in Figure A6 in Appendix A. The weighting coefficients for the power generation cost, active power loss, and total carbon flow rate are assigned as 0.3, 0.2, and 0.5, respectively, based on which TOPSIS decision method is applied. The first five solutions of the evaluation index are shown in Table 3. The solution with the largest evaluation index is selected as the optimal solution, and the corresponding generator output is shown in Table 4.

Table 2. Basic parameter setting of NSGA-III Algorithm.

Population Size	Maximum Number of Iterations	Cross Ratio	Mutation Ratio	Mutation Probability
200	100	0.8	0.2	0.02

Table 3. The top five individuals in the TOPSIS evaluation index.

Order	Power Generation Cost (Million CNY)	Active Network Loss (MW)	Total Carbon Flow Rate ($\times 10^9$ tCO_2/h)	Proximity Index
1	2.440	39.878	1.8007	0.737
2	2.453	43.561	1.7191	0.7262
3	2.443	42.970	1.7490	0.722
4	2.439	43.301	1.7424	0.728
5	2.444	42.580	1.7614	0.725

Figure 3 depicts the power output from each power plant in Scenario 1 and Scenario 2. Figures 4 and 5, respectively, analyze and compare the node carbon potential and the carbon flow rate of each load in and the two scenarios. It is evident that the carbon potential of each node in Scenario 2 is less than or equal to Scenario 1; the carbon flow rate of each load in Scenario 2 is generally lower compared to Scenario 1. However, the green power cannot meet the demand of some of the loads because some of the green power has been used. Therefore, the carbon flow rate in Scenario 2 surpasses that in Scenario 1.

Table 4. The output of power plant under Scenario 2.

Bus	Generation Type	Active Output (MW)	Reactive Output (MVAr)
30	Hydroelectric power generation	1011.07	254.01
31	Coal-fired power generation	316.35	164.31
32	Gas-fired power generation	688.86	206.66
33	Coal-fired power generation	382.40	87.54
34	Wind power generation	495.57	158.96
35	Gas-fired power generation	561.94	192.43
36	Photovoltaic power generation	546.92	92.45
37	Photovoltaic power generation	494.49	39.83
38	Hydroelectric power generation	744.35	16.54
39	Gas-fired power generation	1052.16	85.70

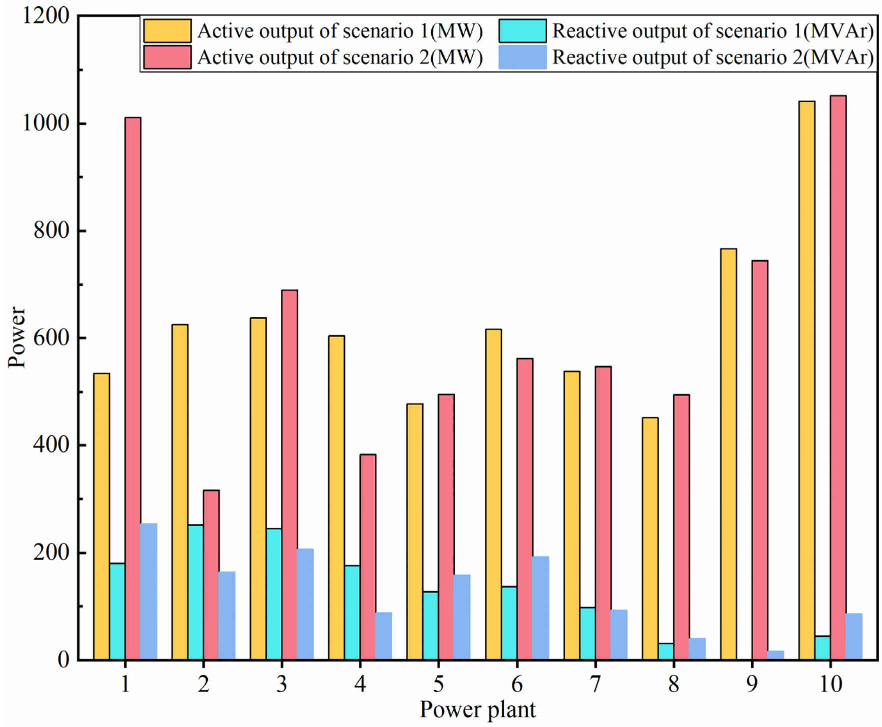

Figure 3. Comparative analysis of power plant output in Scenario 1 and Scenario 2.

From Tables 1 and 4, one can conclude that, compared to Scenario 1, the output of power plants with a high carbon emission intensity in Scenario 2 is significantly reduced. Analyzing the carbon flow rate for each node and load is based on the distribution mechanism and characteristics of carbon emission flow. Considering that the G1, G5, G7, G8, and G9 power plants generate electricity from green energy and have zero carbon emissions, only the carbon flow rate contribution of the G2, G3, G4, G6, and G10 power plants to each node and load is analyzed. The contribution of the power plant to the carbon flow rate of each node and load of the two scenarios are shown in Figures A2–A5 included in Appendix A. It can be seen that there are more nodes with a distribution of carbon emission flow generated by green power in Scenario 2, which indicates that the renewable resources in Scenario 2 are more fully utilized. In addition, the nodes and final flow load of the carbon emission flow from coal-fired power plants in Scenario 2 are less than in Scenario 1, which indicates a reduction in the output ratio of high-carbon-emitting power plants. From Figures A4 and A5 included in Appendix A, to optimize the carbon emissions of load areas 3, 4, and 5, it is necessary to improve the G2 and G3 power plants; to optimize the load areas of 8, 9, 10, 11, and 12, it is necessary to improve the G4 and G6 power plants; and the load 21 area needs to improve the G10 power plant.

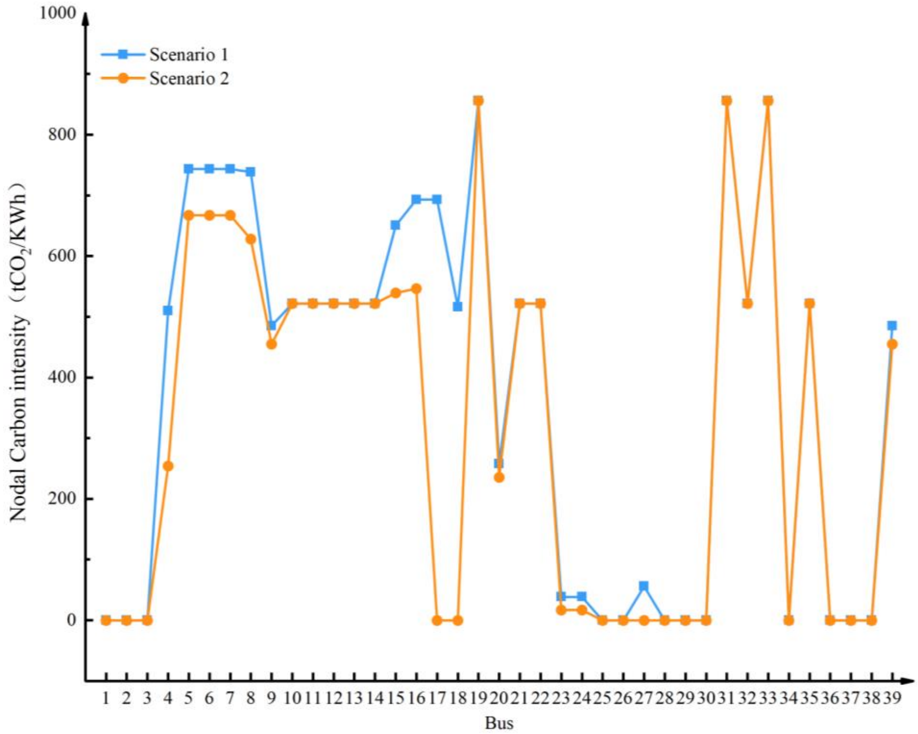

Figure 4. Comparison of node carbon potential in Scenario 1 and Scenario 2. Note: Power injection bus: 30~39; Power consumption bus: 1,3,4,7~9,12,15,16,18,20,21,23~29,31,39.

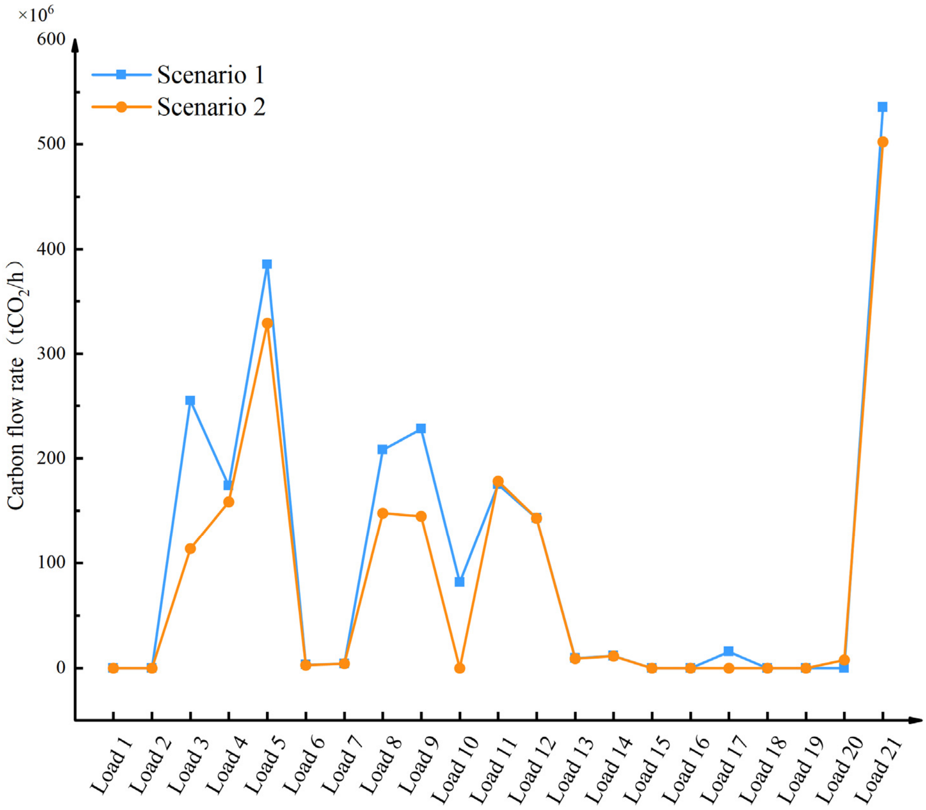

Figure 5. Comparison of load carbon flow rate between Scenario 1 and Scenario 2.

Table 5 compares the power generation cost, real network loss, and total carbon flow rate under the two scenarios. As per the data presented in Table 5, the power generation cost of the system increases by 1.94%, the active network loss increases by 5.78%, and the total carbon flow rate decreases by 20.00%. Compared to Scenario 1, Scenario 2 makes full use of the green power resources in the system and greatly reduces the carbon emissions of the system with a slight increase in power generation costs and active network losses.

Table 5. Comparison of the optimization results of Scenario 1 and Scenario 2.

Scenario	Power Generation Cost (Million CNY)	Active Network Loss (MW)	Total Carbon Flow Rate ($\times$109 tCO_2/h)
1	2.3936	37.698	2.25×109
2	2.4400	39.878	1.80×109

5. Conclusions

In pursuit of both economic and environmental considerations within the power system, this paper introduces an optimal power flow model for the power system, factoring in carbon emission intensity and grounded in the principles of carbon emission flow theory. The model optimizes the cost of power generation, active power loss, and total carbon emission rate, and fully mobilizes low-carbon resources to reduce the carbon emissions of the system with consideration for the economy. In addition, the optimal Pareto front is calculated using the NSGA-III multi-objective optimization algorithm, and the optimal output scheme is acquired via the TOPSIS method. This study yields the subsequent conclusions:

1. The numerical simulation results of the IEEE39 bus system show that, with an increase in the economy cost by only 1.94%, the method proposed can reduce carbon emissions by 20.00%.
2. The optimal Pareto front can provide multiple sets of output schemes, which can be more comprehensive and flexible for each scheduling of various resources.
3. The analysis of the carbon flow rate correlation between power plants, nodes, and loads in the power system can also perform small-scale low-carbon optimization on the loads mounted on a node.

The current research does not consider the intermittency and uncertainty of new energy power generation. Next, it is necessary to predict solar and wind energy resources and study the low-carbon optimal scheduling strategy in different periods of the day. At the same time, it can also increase the energy storage equipment for new energy consumption to improve the utilization rate of renewable resources.

Author Contributions: Methodology, G.W.; validation, H.M. and B.W.; formal analysis, F.M.; writing—original draft preparation, G.W.; writing—review and editing, A.M.A. and H.W. All authors have read and agreed to the published version of the manuscript.

Funding: This work is supported by National Natural Science Foundation of China (52167022), Natural Science Foundation of Qinghai (2022-ZJ-935Q).

Institutional Review Board Statement: Not applicable.

Informed Consent Statement: Not applicable.

Data Availability Statement: Data are contained within the article and Appendix A.

Conflicts of Interest: The authors declare no conflict of interest.

Appendix A

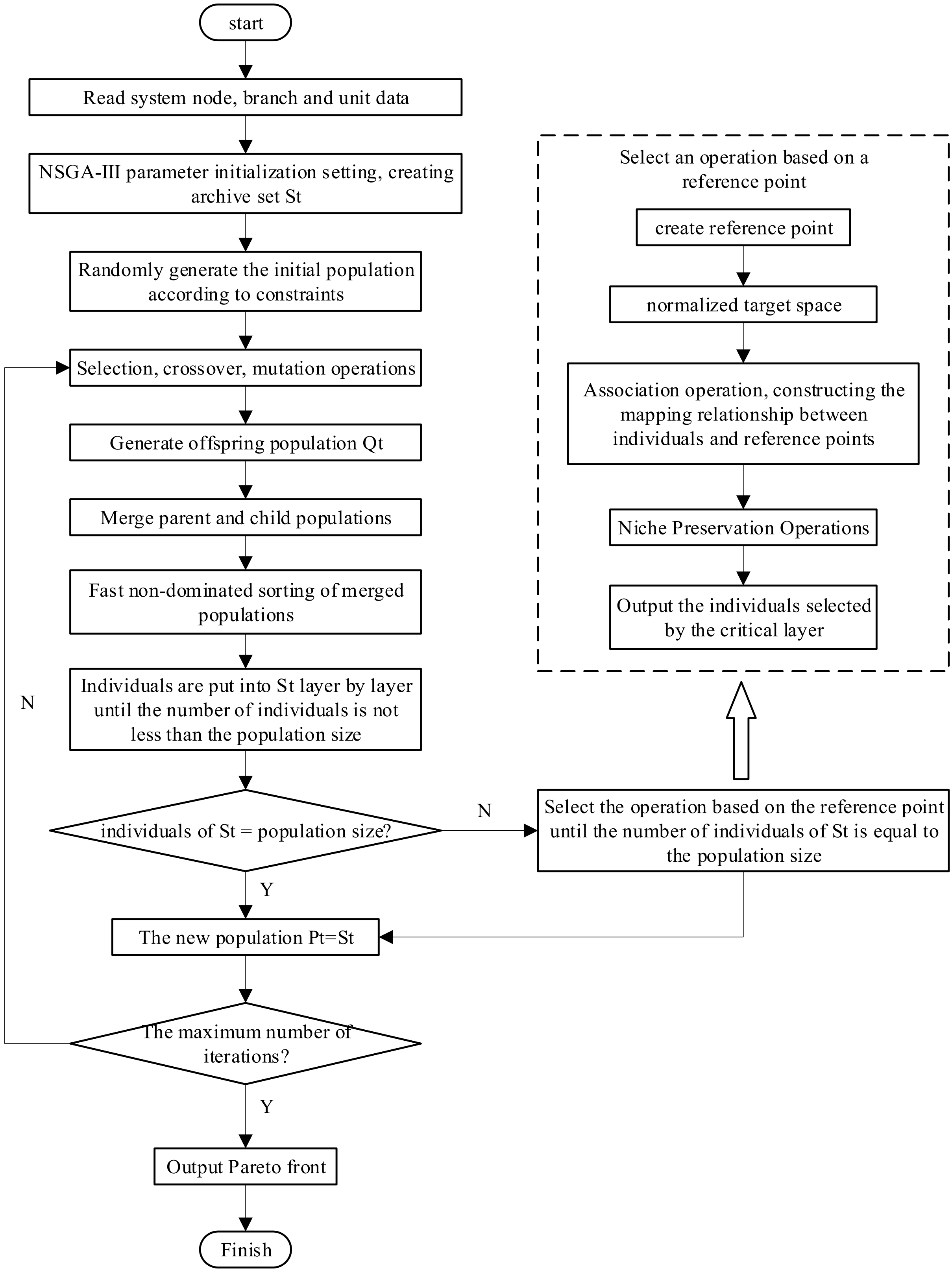

Figure A1. Algorithm flow chart.

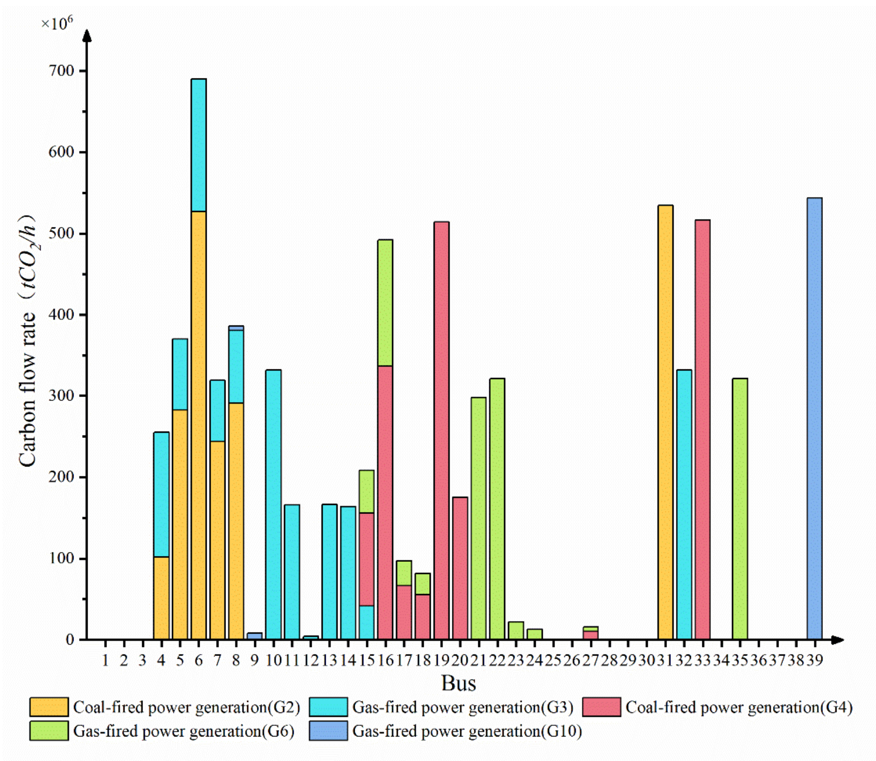

Figure A2. Scenario 1: Power plant—node carbon flow rate correlation analysis.

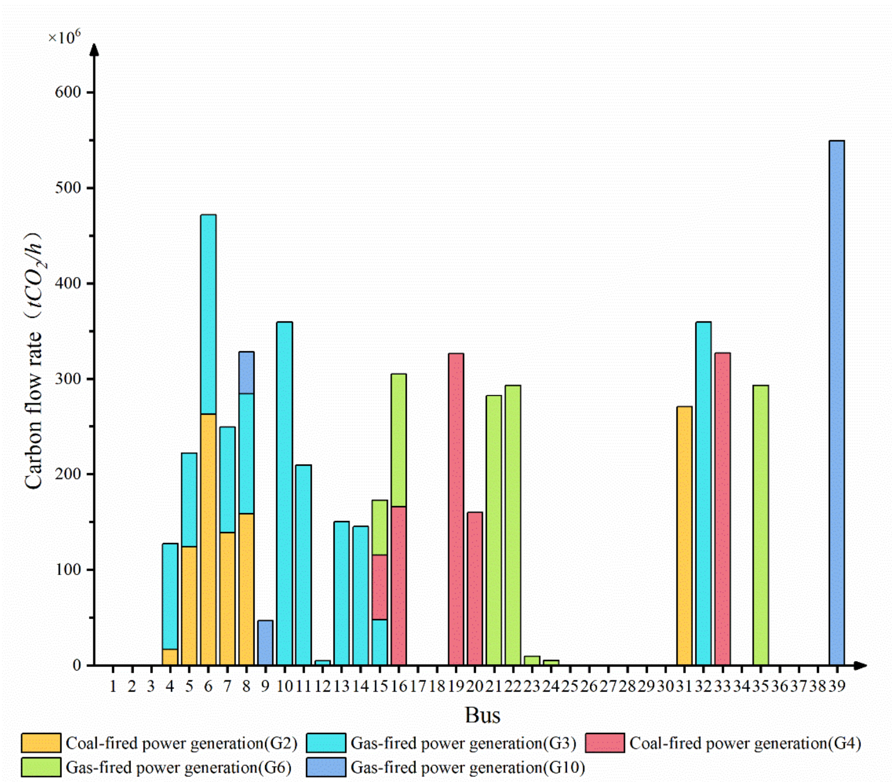

Figure A3. Scenario 2: Power plant—node carbon flow rate correlation analysis.

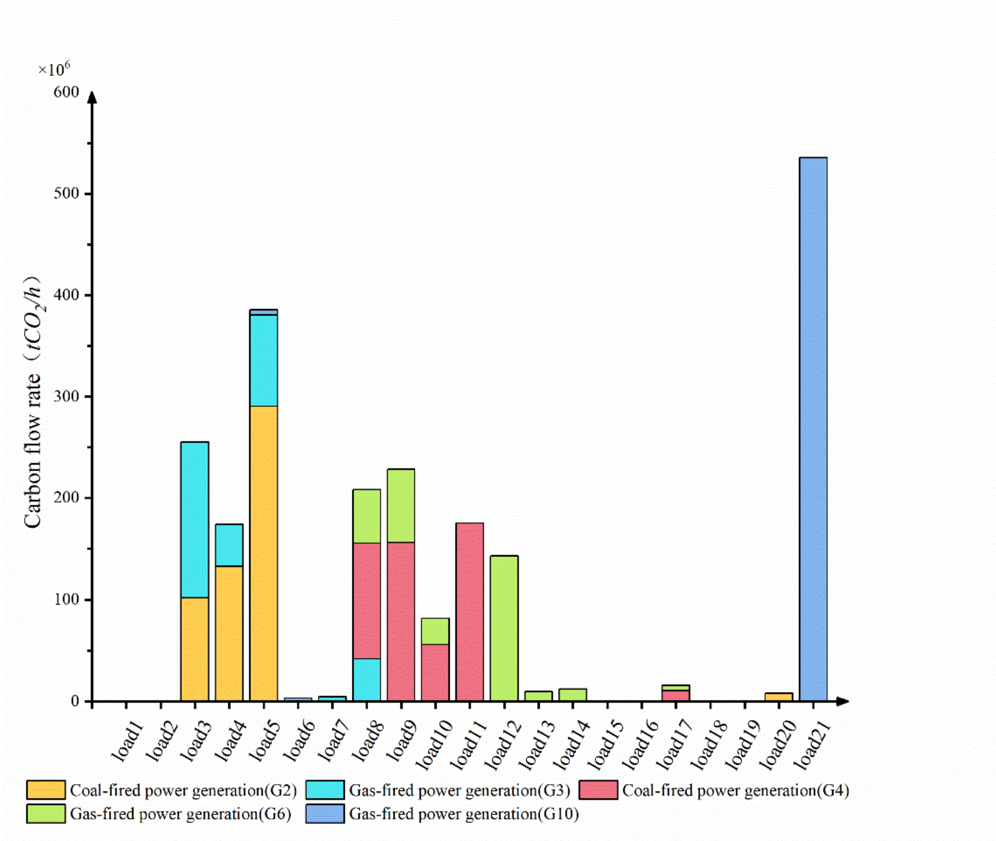

Figure A4. Scenario 1: Power plant—load carbon flow rate correlation analysis.

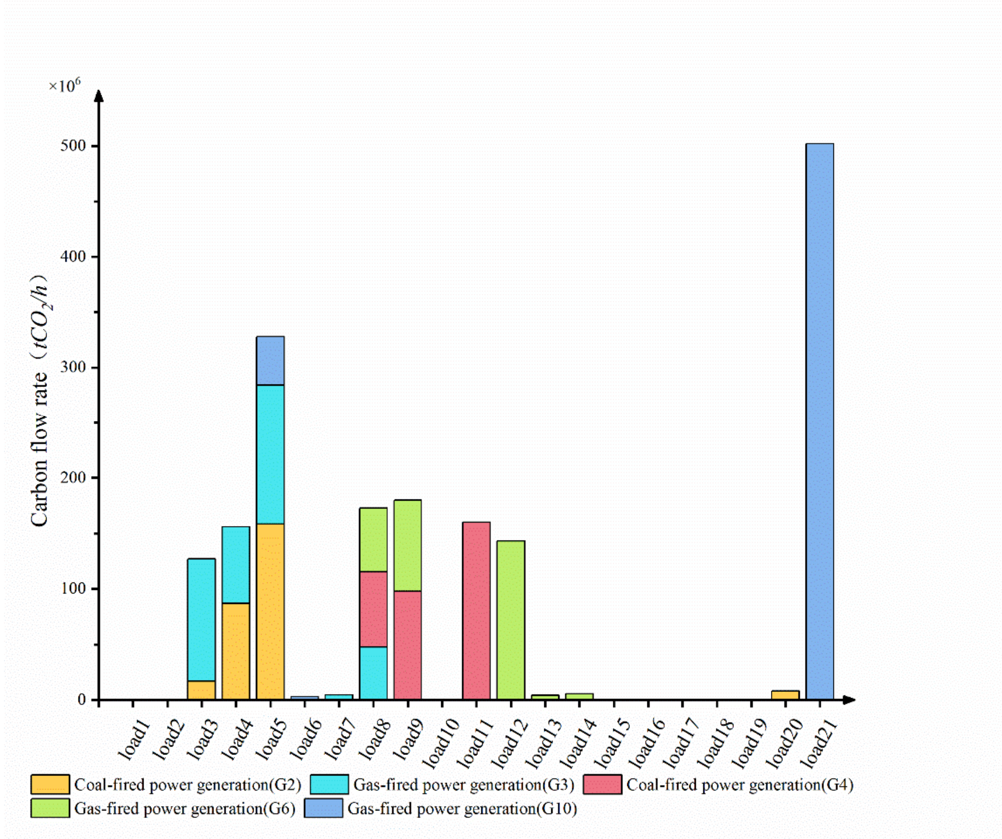

Figure A5. Scenario 2: Power plant—load carbon flow rate correlation analysis.

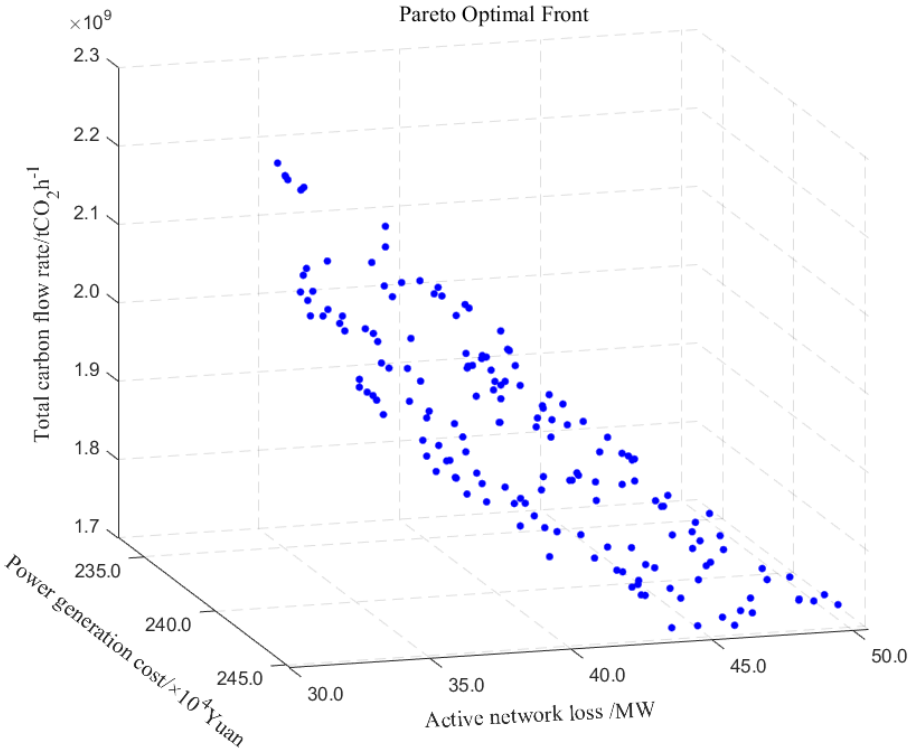

Figure A6. Pareto Optimal Front.

Table A1. Modified IEEE-39 Node System Data for Each Power Plant.

Bus	Generation Type	Active Output (MW)		Reactive Output (MVAr)		Power Generation Cost (Yuan/MWh)	Carbon Intensity (tCO_2/KWh)
		Max	Min	Max	Min		
30	Hydroelectric power generation	1040	0	400	140	335.1	0
31	Coal-fired power generation	646	0	300	−100	260.1	856
32	Gas-fired power generation	725	0	300	150	452.0	522
33	Coal-fired power generation	652	0	250	0	260.1	856
34	Wind power generation	508	0	167	0	460.1	0
35	Gas-fired power generation	687	0	300	−100	452.0	522
36	Photovoltaic power generation	580	0	240	0	387.7	0
37	Photovoltaic power generation	564	0	250	0	387.7	0
38	Hydroelectric power generation	865	0	300	−150	331.5	0
39	Gas-fired power generation	1100	0	300	−100	452.0	522

Table A2. IEEE-39 System Node Data.

Bus	Bus Type	Active Load (MW)	Reactive Load (MVAr)	Voltage Amplitude	
				U_{max}(p.u.)	U_{min}
1	PQ BUS	97.60	44.20	1.06	0.94
2	PQ BUS	0.00	0.00	1.06	0.94
3	PQ BUS	322.00	2.40	1.06	0.94
4	PQ BUS	500.00	184.00	1.06	0.94
5	PQ BUS	0.00	0.00	1.06	0.94
6	PQ BUS	0.00	0.00	1.06	0.94
7	PQ BUS	233.80	84.00	1.06	0.94
8	PQ BUS	522.00	176.60	1.06	0.94
9	PQ BUS	6.50	−66.60	1.06	0.94
10	PQ BUS	0.00	0.00	1.06	0.94
11	PQ BUS	0.00	0.00	1.06	0.94
12	PQ BUS	8.53	88.00	1.06	0.94

Table A2. *Cont.*

Bus	Bus Type	Active Load (MW)	Reactive Load (MVAr)	Voltage Amplitude	
				U_{max}(p.u.)	U_{min}
13	PQ BUS	0.00	0.00	1.06	0.94
14	PQ BUS	0.00	0.00	1.06	0.94
15	PQ BUS	320.00	153.00	1.06	0.94
16	PQ BUS	329.00	32.30	1.06	0.94
17	PQ BUS	0.00	0.00	1.06	0.94
18	PQ BUS	158.00	30.00	1.06	0.94
19	PQ BUS	0.00	0.00	1.06	0.94
20	PQ BUS	680.00	103.00	1.06	0.94
21	PQ BUS	274.00	115.00	1.06	0.94
22	PQ BUS	0.00	0.00	1.06	0.94
23	PQ BUS	247.50	84.60	1.06	0.94
24	PQ BUS	308.60	−92.20	1.06	0.94
25	PQ BUS	224.00	47.20	1.06	0.94
26	PQ BUS	139.00	17.00	1.06	0.94
27	PQ BUS	281.00	75.50	1.06	0.94
28	PQ BUS	206.00	27.60	1.06	0.94
29	PQ BUS	283.50	26.90	1.06	0.94
30	PV BUS	0.00	0.00	1.06	0.94
31	Balance BUS	9.20	4.60	1.06	0.94
32	PV BUS	0.00	0.00	1.06	0.94
33	PV BUS	0.00	0.00	1.06	0.94
34	PV BUS	0.00	0.00	1.06	0.94
35	PV BUS	0.00	0.00	1.06	0.94
36	PV BUS	0.00	0.00	1.06	0.94
37	PV BUS	0.00	0.00	1.06	0.94
38	PV BUS	0.00	0.00	1.06	0.94
39	PV BUS	1104.00	250.00	1.06	0.94

Table A3. IEEE-39 System Branch Data.

Branch	From	To	Resistance (p.u.)	Reactance (p.u.)	Susceptance (p.u.)	Ratio	Max MVA
1	1	2	3.50×10^{-3}	4.11×10^{-2}	0.6987	0	600
2	1	39	1.00×10^{-3}	2.50×10^{-2}	0.75	0	1000
3	2	3	1.30×10^{-3}	1.51×10^{-2}	0.2572	0	500
4	2	25	7.00×10^{-3}	8.60×10^{-3}	0.146	0	500
5	2	30	0.00	1.81×10^{-2}	0	1.025	900
6	3	4	1.30×10^{-3}	2.13×10^{-2}	0.2214	0	500
7	3	18	1.10×10^{-3}	1.33×10^{-2}	0.2138	0	500
8	4	5	8.00×10^{-4}	1.28×10^{-2}	0.1342	0	600
9	4	14	8.00×10^{-4}	1.29×10^{-2}	0.1382	0	500
10	5	6	2.00×10^{-4}	2.60×10^{-3}	0.0434	0	1200
11	5	8	8.00×10^{-4}	1.12×10^{-2}	0.1476	0	900
12	6	7	6.00×10^{-4}	9.20×10^{-3}	0.113	0	900
13	6	11	7.00×10^{-4}	8.20×10^{-3}	0.1389	0	480
14	6	31	0.00	2.50×10^{-2}	0	1.07	1800
15	7	8	4.00×10^{-4}	4.60×10^{-3}	0.078	0	900
16	8	9	2.30×10^{-3}	3.63×10^{-2}	0.3804	0	900
17	9	39	1.00×10^{-3}	2.50×10^{-2}	1.2	0	900
18	10	11	4.00×10^{-4}	4.30×10^{-3}	0.0729	0	600
19	10	13	4.00×10^{-4}	4.30×10^{-3}	0.0729	0	600
20	10	32	0.00	2.00×10^{-2}	0	1.07	900
21	12	11	1.60×10^{-3}	4.35×10^{-2}	0	1.006	500
22	12	13	1.60×10^{-3}	4.35×10^{-2}	0	1.006	500

Table A3. *Cont.*

Branch	From	To	Resistance (p.u.)	Reactance (p.u.)	Susceptance (p.u.)	Ratio	Max MVA
23	13	14	9.00×10^{-4}	1.01×10^{-2}	0.1723	0	600
24	14	15	1.80×10^{-3}	2.17×10^{-2}	0.366	0	600
25	15	16	9.00×10^{-4}	9.40×10^{-3}	0.171	0	600
26	16	17	7.00×10^{-4}	8.90×10^{-3}	0.1342	0	600
27	16	19	1.60×10^{-3}	1.95×10^{-2}	0.304	0	600
28	16	21	8.00×10^{-4}	1.35×10^{-2}	0.2548	0	600
29	16	24	3.00×10^{-4}	5.90×10^{-3}	0.068	0	600
30	17	18	7.00×10^{-4}	8.20×10^{-3}	0.1319	0	600
31	17	27	1.30×10^{-3}	1.73×10^{-2}	0.3216	0	600
32	19	20	7.00×10^{-4}	1.38×10^{-2}	0	1.06	900
33	19	33	7.00×10^{-4}	1.42×10^{-2}	0	1.07	900
34	20	34	9.00×10^{-4}	1.80×10^{-2}	0	1.009	900
35	21	22	8.00×10^{-4}	1.40×10^{-2}	0.2565	0	900
36	22	23	6.00×10^{-4}	9.60×10^{-3}	0.1846	0	600
37	22	35	0.00	1.43×10^{-2}	0	1.025	900
38	23	24	2.20×10^{-3}	3.50×10^{-2}	0.361	0	600
39	23	36	5.00×10^{-4}	2.72×10^{-2}	0	1	900
40	25	26	3.20×10^{-3}	3.23×10^{-2}	0.531	0	600
41	25	37	6.00×10^{-4}	2.32×10^{-2}	0	1.025	900
42	26	27	1.40×10^{-3}	1.47×10^{-2}	0.2396	0	600
43	26	28	4.30×10^{-3}	4.74×10^{-2}	0.7802	0	600
44	26	29	5.70×10^{-3}	6.25×10^{-2}	1.029	0	600
45	28	29	1.40×10^{-3}	1.51×10^{-2}	0.249	0	600
46	29	38	8.00×10^{-4}	1.56×10^{-2}	0	1.025	1200

References

1. Xi, J. Speech at the General Debate of the 75th United Nations General Assembly. *People's Daily*, 23 September 2020; edition 003. [CrossRef]
2. Kang, C.; Du, E.; Li, Y.; Zhang, N.; Chen, Q.; Guo, H.; Wang, P. 'Carbon perspective' of new power systems: Scientific issues and research framework. *Power Syst. Technol.* **2022**, *46*, 821–833. [CrossRef]
3. Tianhua, M.; Qiaoyan, B.; Jun, X.; Deqiang, G. Low-carbon power dispatching and benefit allocation considering carbon emission allowance. *Autom. Electr. Power Syst.* **2016**, *40*, 49–55.
4. Hao, X.; Kong, Y. Analysis of the low-carbon transformation path of the power sector under the goal of carbon neutrality. *Compr. Util. Resour. China* **2022**, *40*, 179–182.
5. Guo, X.; Lou, S.; Wu, Y.; Wang, Y. Low-carbon Operation of Combined Heat and Power Integrated Plants Based on Solar-assisted Carbon Capture. *J. Mod. Power Syst. Clean Energy* **2022**, *10*, 1138–1151. [CrossRef]
6. Liu, H.; Wang, X.; Zuo, D.; Wang, Y. Research on low-carbon transformation of power system under the background of double carbon. *Electr. Appl. Ind.* **2023**, *268*, 40–44.
7. Xu, B.; Zhang, G.; Li, K.; Li, B.; Chi, H.; Yao, Y.; Fan, Z. Reactive power optimization of a distribution network with high-penetration of wind and solar renewable energy and electric vehicles. *Prot. Control Mod. Power Syst.* **2022**, *7*, 801–813. [CrossRef]
8. Zhang, Y.; Xie, X.; Fu, W.; Chen, X.; Hu, S.; Zhang, L.; Xia, Y. An Optimal Combining Attack Strategy Against Economic Dispatch of Integrated Energy System. *IEEE Trans. Circuits Syst. II Express Briefs* **2023**, *70*, 246–250. [CrossRef]
9. Li, K.; Han, X. Distributed algorithm of real-time optimal power flow for distribution network with distributed energy resource. *Autom. Electr. Power Syst.* **2020**, *44*, 54–61.
10. Zhang, N.; Zhang, K.; Li, Q.; Liu, J.; Zhao, J.; Sun, G. Optimal power flow calculation of power system containing TCPST based on improved MCCIPM. *Electr. Power Eng. Technol.* **2021**, *40*, 144–150. [CrossRef]
11. Zhu, J.P.; Huang, Y.; Ma, L. Assessment on Distributed Generation Accommodation Capability for Distribution Network Based on Uncertain Optimal Power Flow. *Autom. Electr. Power Syst.* **2022**, *46*, 46–54.
12. Riaz, M.; Hanif, A.; Masood, H.; Khan, M.A.; Afaq, K.; Kang, B.G.; Nam, Y. An Optimal Power Flow Solution of a System Integrated with Renewable Sources Using a Hybrid Optimizer. *Sustainability* **2021**, *13*, 13382. [CrossRef]
13. Wang, C.; Zhu, J.; Li, G.; Zhang, B. Low-Carbon Power Dispatch Based on Evolutionary Algorithm with Adaptive Weight. In Proceedings of the 2011 Asia-Pacific Power and Energy Engineering Conference, Wuhan, China, 25–28 March 2011; pp. 1–4. [CrossRef]
14. Zhang, C.; Yuan, Y.; Zhang, X.; Cao, Y.; Zhang, M. A Day-Ahead Scheduling Planning Model for Wind Power Systems Considering the Impact of Carbon Emission Quotas. *Power Syst. Technol.* **2014**, *38*, 2114–2120. [CrossRef]

15. Han, H.; Wei, T.; Wu, C.; Xu, X.; Zang, H.; Sun, G.; Wei, Z. A Low-Carbon Dispatch Strategy for Power Systems Considering Flexible Demand Response and Energy Storage. *Front. Energy Res.* **2022**, *10*, 883602. [CrossRef]
16. Li, J.; He, X.; Li, W.; Zhang, M.; Wu, J. Low-carbon optimal learning scheduling of the power system based on carbon capture system and carbon emission flow theory. *Electr. Power Syst. Res.* **2023**, *218*, 109215. [CrossRef]
17. Dong, Y.; Shan, X.; Yan, Y.; Leng, X.; Wang, Y. Architecture, Key Technologies and Applications of Load Dispatching in China Power Grid. *J. Mod. Power Syst. Clean Energy* **2022**, *10*, 316–327. [CrossRef]
18. Zhong, H.; Zhang, L.; Dong, X. Bi-level emission reduction model of the hybrid power market based on Carbon Emission Flow Theory and source-load coordination. *Appl. Sci.* **2023**, *13*, 9100. [CrossRef]
19. Jiang, G.; Wang, B.; Xu, P. A method for power flow calculation and optimal dispatch of gas–thermal–electricity multi energy system considering unit commitment. *Energy Rep.* **2023**, *9*, 718–727. [CrossRef]
20. Fakih, S.; Mabrouk, M.T.; Batton-Hubert, M.; Lacarrière, B. Bi-level and multi-objective optimization of renewable energy sources and storage planning to support existing overloaded electricity grids. *Energy Rep.* **2023**, *10*, 1450–1466. [CrossRef]
21. Chen, H.; Mao, W.; Zhang, R.; Yu, W. Power System Source-Load Coordinated Low-Carbon Optimal Dispatch Based on Carbon Emission Flow Theory. *Power Syst. Prot. Control* **2021**, *49*, 1–11. [CrossRef]
22. Zhou, T.; Kang, C.; Xu, Q.; Chen, Q. Preliminary Theoretical Investigation on Power System Carbon Emission Flow. *Autom. Electr. Power Syst.* **2012**, *36*, 38–43+85.
23. Zhou, T.; Kang, C.; Xu, Q.; Chen, Q. Preliminary Investigation on a Method for Carbon Emission Flow Calculation of Power System. *Autom. Electr. Power Syst.* **2012**, *36*, 44–49.
24. Li, Y.; Liu, Q.; Zhang, Z.; Liu, J. Calculation method of carbon emission flow based on grid power distribution. *Power Grid Technol.* **2017**, *41*, 840–844. [CrossRef]
25. Zhou, T.; Kang, C.; Xu, Q.; Chen, Q.; Xin, J.; Wu, Y. Analysis on Distribution Characteristics and Mechanisms of Carbon Emission Flow in Electric Power Network. *Autom. Electr. Power Syst.* **2012**, *36*, 39–44.
26. Cao, D.; Hu, W.; Xu, X.; Wu, Q.; Huang, Q.; Chen, Z.; Blaabjerg, F. Deep reinforcement learning based approach for optimal power flow of distribution networks embedded with renewable energy and storage devices. *J. Mod. Power Syst. Clean Energy* **2021**, *9*, 1101–1110. [CrossRef]
27. Yang, N.; Dong, Z.; Wu, L.; Zhang, L.; Shen, X.; Chen, D.; Zhu, B.; Liu, Y. A Comprehensive Review of Security-constrained Unit Commitment. *J. Mod. Power Syst. Clean Energy* **2022**, *10*, 562–576. [CrossRef]
28. Nan, Y.; Di, Y.; Zheng, Z.; Jiazhan, C.; Daojun, C.; Xiaoming, W. Research on Modelling and Solution of Stochastic SCUC under AC Power Flow Constraints. *IET Gener. Transm. Distrib.* **2018**, *12*, 3618–3625. [CrossRef]
29. Zhu, M.; Xu, C.; Dong, S.; Tang, K.; Gu, C. An integrated multi-energy flow calculation method for electricity-gas-thermal integrated energy systems. *Prot. Control Mod. Power Syst.* **2021**, *6*, 65–76. [CrossRef]
30. Yang, N.; Qin, T.; Wu, L.; Huang, Y.; Huang, Y.; Xing, C.; Zhang, L.; Zhu, B. A multi-agent game based joint planning approach for electricity-gas integrated energy systems considering wind power uncertainty. *Electr. Power Syst. Res.* **2022**, *204*, 107673. [CrossRef]
31. Deb, K.; Jain, H. An evolutionary many-objective optimization algorithm using reference-point-based nondominated sorting approach, Part I: Solving Problems with Box Constraints. *IEEE Trans. Evol. Comput.* **2014**, *18*, 577–601. [CrossRef]
32. Zhang, R.; Feng, X.; Ma, G. Production scheduling and transportation optimization of prefabricated components considering carbon emissions based on NSGA-III algorithm. *J. Eng. Manag.* **2023**, *37*, 153–158. [CrossRef]
33. Gu, Q.; Luo, J.; Li, X. Multi-objective evolutionary algorithm based on niche. *Comput. Eng. Appl.* **2023**, *59*, 126–139.
34. Zhao, Q.; Bai, Q.; Nie, K.; Wang, H.; Zeng, X. Multi-objective optimal allocation of regional water resources based on NSGA-III algorithm and TOPSIS decision. *J. Drain. Irrig. Mech. Eng.* **2022**, *40*, 1233–1240.
35. Hwang, C.-L.; Lai, Y.-J.; Liu, T.-Y. A new approach for multiple objective decision making. *Comput. Oper. Res.* **1993**, *20*, 889–899. [CrossRef]
36. Xu, P.; Fu, W.; Lu, Q.; Zhang, S.; Wang, R.; Meng, J. Stability analysis of hydro-turbine governing system with sloping ceiling tailrace tunnel and upstream surge tank considering nonlinear hydro-turbine characteristics. *Renew. Energy* **2023**, *210*, 556–574. [CrossRef]
37. Zhang, Z.; Ban, M.; Guo, D.; Chen, Q.; Jiang, H. A model for Carbon dioxide emission characteristics of coal-fired units for environmental-economic dispatch research. *J. Shanghai Jiao Tong Univ.* **2021**, *55*, 1663–1672. [CrossRef]
38. Zhang, S. Research on the Economics of Wind Power Project Investment Based on KWH Cost and Development Potential—Taking Fujian Luoyuan Bay Wind Farm as an Example. *China Price Superv. Anti Monop.* **2023**, 69–72.
39. Li, X.; Gao, Y. Application status and benefit analysis of hub airport PV power generation project. *Sol. Energy* **2022**, 5–11. [CrossRef]
40. Zhang, X.; Liang, J.; Zhao, C. Low-carbon power planning with gas-fired units based on carbon trading. *J. Sol. Energy Sin.* **2020**, *41*, 92–98.